Journal of Electronic Imaging

JElectronicImaging.org

Tone-dependent error diffusion based on an updated blue-noise model

Yik-Hing Fung
Yuk-Hee Chan

SPIE. IS&T imaging.org

Downloaded From: https://www.spiedigitallibrary.org/journals/Journal-of-Electronic-Imaging on 09 Nov 2022
Terms of Use: https://www.spiedigitallibrary.org/terms-of-use

Journal of Electronic Imaging 25(1), 013013 (Jan/Feb 2016)

Tone-dependent error diffusion based on an updated blue-noise model

Yik-Hing Fung and Yuk-Hee Chan*
Hong Kong Polytechnic University, Department of Electronic and Information Engineering, Hung Hom, Kowloon, Hong Kong

Abstract. The conventional blue-noise model that specifies the desired noise characteristics of an ideal halftone has been updated recently, and simulation results showed that the updated model can serve as a better guideline for developing halftone algorithms. At the moment, only a feature-preserving multiscale error diffusion-based algorithm was developed based on the updated noise model. As the algorithm does not support real-time applications, a tone-dependent error diffusion (TDED) algorithm is developed based on the updated noise model. To support the proposed TDED algorithm, we optimize a diffusion filter and a quantizer threshold for each possible input gray level based on the updated noise model, such that the algorithm can adapt its diffusion filter and quantizer according to the input intensity value of a pixel to produce a halftone. Simulation results showed that the proposed TDED algorithm can successfully produce halftones bearing the desired noise characteristics as specified by the updated noise model. As a consequence, it provides better performance than conventional error diffusion-based algorithms in terms of various measures including radially averaged power spectrum density and anisotropy. When processing real images, it can eliminate directional artifacts, regular structure patterns, and unintended sharpening effects in its halftoning outputs. *© 2016 SPIE and IS&T* [DOI: 10.1117/1.JEI.25.1.013013]

Keywords: error diffusion; tone-dependent error diffusion; halftoning; printing; blue noise.

Paper 15679 received Sep. 2, 2015; accepted for publication Dec. 15, 2015; published online Jan. 25, 2016.

1 Introduction

Digital halftoning is a process that converts a continuous tone image to a binary image, and it has been widely exploited in various applications. Halftoning techniques can roughly be classified into three categories: screening,[1] error diffusion,[2–5] and iterative optimization.[6–8] Among them, screening requires the lowest computational complexity but it is hard to produce halftones of high quality. By contrast, iterative optimization can optimize the quality in terms of a specific measure at a cost of complexity. Error diffusion is good for most of the applications as it can produce halftones of fairly good quality at an affordable computational complexity such that real-time halftoning can be realized. Due to its popularity and practicality in various applications in different areas, how to improve error diffusion is still an active research problem.

In practice, a conventional error diffusion algorithm can be realized as follows. Image pixels are scanned along a predefined path. The intensity value (a.k.a. gray level) of each of them is quantized to either 0 or 1 (i.e., the minimum or the maximum allowable output intensity levels) with a threshold. The quantization error is then diffused to the unprocessed neighboring pixels before the next pixel is processed. Here, without loss of generality, we assume that the input intensity value of a pixel is bounded in [0, 1].

In the simplest mode of the realization, pixels are raster-scanned, pixel values are quantized with a fixed threshold equal to 0.5, and the quantization error is diffused with a nonadaptive causal diffusion filter. This simple arrangement is unable to cope with the different possible input scenarios and hence, one can easily find some artifacts in the output of a conventional error diffusion algorithm. These artifacts include (1) worm artifacts that appear at highlight and shadow regions, (2) unintended sharpening effects caused by the diffusion filter, and (3) regular structure patterns that appear at certain gray levels near the midtone. The mixture of these artifacts can be very visible for some ranges of input gray levels.

To reduce the artifacts, various modifications to the aforementioned simple arrangement have been proposed based on the following directions. The first direction is to change the scanning path such that pixels are not processed in a fixed order to create a directional bias in the diffusion of error.[9–16] The second one is to adjust the quantizer threshold according to the input so as to compensate for the sharpening effect.[17–22] The third one is to make the error diffusion filter adaptive to the local spatial characteristics of the image so as to remove the structure patterns.[4,5,23–33] Among the modifications based on the first two directions, the serpentine scanning scheme suggested in Ref. 9 and the threshold modulation scheme proposed in Ref. 18 are, respectively, considered as effective means for tackling the worm artifacts and the sharpening effect of error diffusion.

For the modification of error diffusion filter, it is possible to adjust either the filter support or the filter coefficients based on different criteria. Among them, tone-dependent error diffusion (TDED) has drawn a number of attentions.[29,31–34] The idea of TDED is to use different diffusion filters for different gray levels of an input pixel. Shiau and Fan[23] developed a set of diffusion filters based on this idea to reduce the worm artifacts. Eschbach[29] suggested using a larger filter for highlight and shadow regions but a smaller

*Address all correspondence to: Yuk-Hee Chan, E-mail: enyhchan@polyu.edu.hk

1017-9909/2016/$25.00 © 2016 SPIE and IS&T

Downloaded From: https://www.spiedigitallibrary.org/journals/Journal-of-Electronic-Imaging on 09 Nov 2022
Terms of Use: https://www.spiedigitallibrary.org/terms-of-use

filter for midtones. Ostromoukhov[31] optimized a set of error diffusion filters for some key gray levels based on a blue noise model[16] and then derived filters for other gray levels with interpolation based on the optimized filters. Instead of optimizing the filters with a blue-noise model, Li and Allebach[32] proposed a TDED scheme in which the coefficient values of the diffusion filter for a particular gray level are optimized based on a human visual system model. Hwang et al.[33] improved the performance of Ref. 31 by optimizing one error diffusion filter for each gray level based on a blue-noise model. Tone-dependent threshold modulation was introduced to Ostromoukhov's scheme[31] by Zhou and Fang.[34]

It is generally accepted that a halftone of good visual quality should bear the blue noise characteristics. To quantize the evaluation criteria, Ulichney[16] suggested a blue-noise model for describing the desired noise characteristics of an ideal halftone. In practice, a binary halftone can be treated as a picture having dots on a background. By considering that dots are actually put on grid points in digital halftoning, Ulichney's blue noise model was revised by Lau and Ulichney[35] to tackle the aliasing problem that occurs when the input gray levels are midtones. Conceptually, the revised model requests that the noise spectra for any input gray levels are radially symmetric. It was found that halftones with the revised noise characteristics can maintain its grid defiance illusion fundamental to the spirit of the blue noise model.[35]

Fung and Chan[36] revised Lau and Ulichney's blue-noise model further by taking the stochastic nature of the dot distribution in a stochastic halftone into account. After the revision, the model requests that the noise spectra for any input gray levels are isotropic rather than just radially symmetric. This property eliminates the potential artifacts caused by directional hysteresis and aliasing problems.

For reference purpose, the three different versions of blue-noise models proposed in Refs. 16, 35, and 36 are, respectively, referred to as BNM, BNM_1, and BNM_2 hereafter.

To produce a halftone that bears the noise characteristics specified by BNM_2, a halftoning algorithm should introduce a minimum degree of dot clustering when halftoning midtone levels. In principle, the success relies on whether it can effectively control the average cluster size and the average distance among neighboring dot clusters. It is not an easy task for conventional error diffusion techniques, as whether these parameters can be tuned flexibly is basically not considered in their development. At the moment, only one halftoning algorithm is reported to be able to achieve the goal and it is developed based on feature-preserving multiscale error diffusion (FMED).[36] By considering that FMED is a time-consuming iterative algorithm and not suitable for real-time applications, it would be a natural move to explore if we can develop an error diffusion-based algorithm that can produce halftones of the same noise characteristics.

In this paper, a new TDED algorithm is proposed for producing halftones bearing the noise characteristics specified by BNM_2. This algorithm processes image pixels sequentially with serpentine scanning. When processing a pixel, it selects a quantizer threshold and a diffusion filter from respective sets of optimized candidates according to the input gray level of the pixel. To support the algorithm, for each potential input gray level, a diffusion filter and a quantizer threshold, respectively, are optimized. The former is optimized to make the resultant halftone possess the desired noise characteristics that target for eliminating directional artifacts and regular structure patterns while the latter is optimized to compensate for the sharpening effect of a diffusion filter.

The organization of this paper is as follows. Section 2 reviews the original error diffusion algorithm. Section 3 reviews the different blue noise models that describe the desired noise characteristics of a halftone. In Sec. 4, based on a recently proposed blue noise model,[36] we optimize a set of diffusion filters to support TDED. This results in a new TDED algorithm. Section 5 shows how the proposed TDED algorithm removes the unwanted sharpening effect introduced by typical diffusion filters by adjusting the quantizer threshold based on the input pixel intensity value. In Sec. 6, a detailed analysis on the performance of the proposed TDED algorithm in terms of various measures is given. Simulation results on real images are provided for comparison in Sec. 7. Finally, a conclusion is given in Sec. 8.

2 Review of Error Diffusion

Consider the case that one wants to halftone a gray level image $\mathbf{X}$ to produce a binary image $\mathbf{H}$. Image $\mathbf{X}$ is normalized such that its maximum and minimum intensity values are 1 and 0, respectively.

The working principle of a conventional error diffusion system is shown in Fig. 1. Here, $x(m,n)$ and $h(m,n)$ are, respectively, the intensity values of pixel (m,n) of image $\mathbf{X}$ and image $\mathbf{H}$. The quantization function $Q(\cdot)$ of the quantizer is given as

$$Q(u(m,n),t_0)=\begin{cases}1 & \text{if } u(m,n)\geq t_0\\ 0 & \text{else}\end{cases}, \tag{1}$$

where t_0 is a threshold and is set to 0.5, in general, when $x(m,n)\in[0,1]$. The input to the quantizer is obtained by

$$u(m,n)=x(m,n)-\left(\sum_{(k,l)\in S}w(k,l)e(m-k,n-l)\right), \tag{2}$$

where $e(m,n)$ is the quantization error given as

$$e(m,n)=h(m,n)-u(m,n) \tag{3}$$

and $w(k,l)$ is the coefficient value of diffusion filter $\mathbf{w}$ at position (k,l). In practice, we have $\sum_{(k,l)\in S}w(k,l)=1$ to preserve the local energy. S is a causal filter support with respect to the processing path such that only quantization errors of previously processed pixels are diffused into current position. Note that $(0,0)\notin S$.

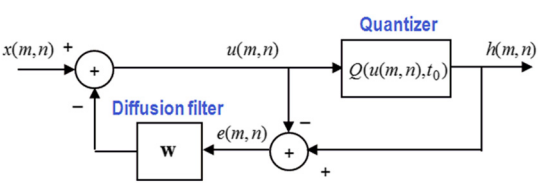

Fig. 1 Conventional error diffusion.

Downloaded From: https://www.spiedigitallibrary.org/journals/Journal-of-Electronic-Imaging on 09 Nov 2022
Terms of Use: https://www.spiedigitallibrary.org/terms-of-use

3 Review of Blue Noise Models

The basic idea of blue noise halftoning is that a good quality halftone should have a frequency spectrum that only contains high-frequency random noise. To quantify this idea, BNM[16] suggests that dots appearing in the halftoning output of a constant gray level patch should be isolated and their distribution should be aperiodic, homogeneous, and isotropic. Halftones with such a dot arrangement have a radially symmetric spectrum. In addition, the spectral energy concentrates at a particular radial frequency defined as

$$f_B(g) = \begin{cases} \sqrt{g} & \text{for } 0 \le g \le 1/2 \\ \sqrt{1-g} & \text{for } 1/2 < f \le 1 \end{cases}, \tag{4}$$

where g is the gray level of the patch. This frequency is referred to as the principal radial frequency of gray level g, and there should be minimal energy in the frequency band below the principal radial frequency. This forms the signature characteristics of a blue-noise spectrum.

Lau and Ulichney[35] showed that, when the ideal blue noise model[16] is applied to practical cases in which dots can only be put on grid points, the desired principal radial frequencies for $0.25 \le g \le 0.75$ can only be achieved by introducing more diagonal correlations among dots. However, the added correlation can create undesired visible patterns in which dots are more likely to occur along diagonal. This violates the isotropic requirement of the conventional blue noise model[16] and introduces directional artifacts. In view of this, Lau and Ulichney proposed a modification of BNM to maintain the isotropy of the spectrum for $0.25 \le g \le 0.75$ by keeping the principal radial frequency constant after it reaches 0.5 as follows:

$$f_B(g) = \begin{cases} \sqrt{g} & \text{for } 0 \le g \le 1/4 \\ 0.5 & \text{for } 1/4 < g \le 3/4 \\ \sqrt{1-g} & \text{for } 3/4 < g \le 1 \end{cases}. \tag{5}$$

This can be achieved by clustering minority dots and then controlling the average distance between the centers of two neighboring dot clusters to be 2 when $0.25 \le g \le 0.75$ occurs.

Fung and Chan[36] observed that neither BNM nor BNM_1 takes the stochastic nature of the dot distribution into account. This nature introduces considerable amount of noise energy in a narrow frequency band surrounding the principal radial frequency. This frequency band [referred to as $B(f_B(g))$ hereafter] can cause aliasing problem, as shown in Fig. 2(c), even if we clip $f_B(g)$ to 0.5 for $0.25 \le g \le 0.75$, as requested by BNM_1.

In view of this, Fung and Chan[36] proposed a new blue noise model BNM_2 in which $f_B(g)$ is clipped to a value <0.5 instead to make the upper bound of $B(f_B(g))$ just touches the boundary of the baseband in the extreme case, as shown in Fig. 2(d). The aliasing problem can then be eliminated and the spectrum can still be isotropic for $0.25 \le g \le 0.75$. In formulation, the preferred principal radial frequency in BNM_2 is given as

$$f_B(g) = \begin{cases} \sqrt{g} & \text{for } 0 \le g \le 1/4 - \delta \\ f(g) & \text{for } 1/4 - \delta \le g \le 0.5 \\ f_B(1-g) & \text{for } 0.5 < g \le 1 \end{cases}, \tag{6}$$

where $f(g)$ is a monotonic increasing function that gradually increases from $\sqrt{0.25-\delta}$ to $0.5-\Delta$. Parameter Δ is the absolute difference between the upper bound of frequency band $B(f_B(g))$ and principal radial frequency $f_B(g)$, and δ is a positive empirical parameter. Readers who are interested in the model can refer to Ref. 36 for more details.

Figures 2(b)–2(d) highlight the conceptual difference of the three noise models in the power spectra of their desired halftoning outputs for a constant gray level patch when $0.25 \le g \le 0.75$. When g is out of this range, all models prefer halftoning outputs of the same characteristics, as shown in Fig. 2(a).

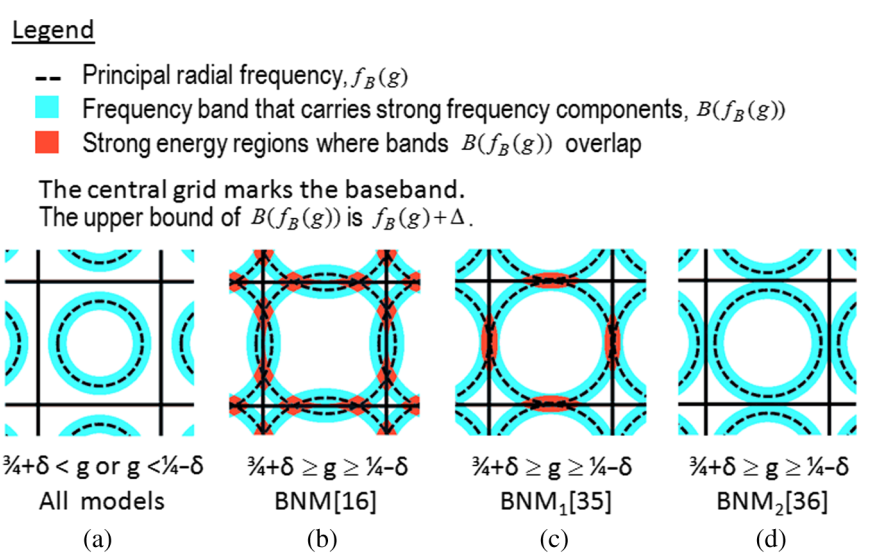

Fig. 2 Power spectra of the desired halftones of a constant patch under different blue noise models: (a) all models, when $3/4+\delta < g$ or $g < 1/4-\delta$; (b) BNM,[16] when $3/4+\delta \ge g \ge 1/4-\delta$; (c) BNM_1,[35] when $3/4+\delta \ge g \ge 1/4-\delta$; and (d) BNM_2,[36] when $3/4+\delta \ge g \ge 1/4-\delta$. In each plot, the center square marks the baseband, the bandwidth of which in a direction is normalized to 0.5.

Downloaded From: https://www.spiedigitallibrary.org/journals/Journal-of-Electronic-Imaging on 09 Nov 2022
Terms of Use: https://www.spiedigitallibrary.org/terms-of-use

4 Optimization of Error Diffusion Filters

The proposed TDED algorithm requires a set of optimized diffusion filters for handling different input gray levels. In this section, we develop a g-dependent objective function based on noise model BNM_2 and then optimize one diffusion filter for each possible gray level g by maximizing the corresponding objective function.

4.1 *Objective Function for Each Gray Level*

According to the noise models,[16,35,36] a well-formed halftone of a constant patch of gray level g should consist of an isotropic field of dots or dot clusters with an average separation distance $\lambda_B(g)$. This average distance is called the principal radial wavelength and its reciprocal provides the principal radial frequency of the halftone.

In reality, dots or dot clusters are separated with a distance around $\lambda_B(g)$ due to the stochastic nature of their distribution. Let the center-to-center distance between two neighboring dots or dot clusters be d. Without loss of generality, we can assume that the distribution of d is Gaussian with mean $\lambda_B(g)$ and most values of d fall in the range of $[\lambda_B(g)(1-\alpha), \lambda_B(g)(1+\alpha)]$, where α is a positive value. The variation of d in $[\lambda_B(g)(1-\alpha), \lambda_B(g)(1+\alpha)]$ introduces strong frequency components in a frequency band denoted as $\Phi_B(g)$, the radial frequencies of which are bounded by $[f_B(g)/(1+\alpha), f_B(g)/(1-\alpha)]$. In formulation, we have

$$\Phi_B(g) = \{(u,v) | f_B(g)/(1+\alpha) < \sqrt{u^2+v^2} < f_B(g)/(1-\alpha)\}. \tag{7}$$

According to the noise models, noise energy should concentrate at principal radial frequency $f_B(g)$ and hence, α should be a small value to keep $\Phi_B(g)$ narrow.

Equation (6) shows the preferred principal radial frequency for a particular g in BNM_2. The function $f(g)$ in Eq. (6) is a monotonic increasing function bounded by $\sqrt{0.25-\delta}$ and $0.5-\Delta$. According to Ref. 36, the value difference between $\sqrt{0.25-\delta}$ and $0.5-\Delta$ is very small and it should be empirically derived based on the halftoning output of a specific halftoning algorithm. As halftoning output is algorithm dependent and there is no way to get the halftoning results of the algorithm to be developed before its diffusion filters are defined, we are forced to simplify $f(g)$ to constant $0.5-\Delta$. Then, from Eq. (6), we have $f_B(1/4-\delta) = \sqrt{1/4-\delta} = 0.5-\Delta$. Equation (6) can hence be rewritten as

$$f_B(g) = \begin{cases} \sqrt{g} & \text{for } 0 \le g \le (0.5-\Delta)^2 \\ 0.5-\Delta & \text{for } (0.5-\Delta)^2 \le g \le 0.5 \\ f_B(1-g) & \text{for } 0.5 < g \le 1 \end{cases}. \tag{8}$$

According to model BNM_2, $f_B(g)$ should be bounded by $0.5-\Delta$ to make sure that there is no aliasing. In view of the nature of $B(f_B(g))$ and $\Phi_B(g)$, the two frequency bands are considered identical when deriving our objective function for optimizing the diffusion filters. Their upper bounds should then be equal. At the extreme case, where $f_B(g) = 0.5-\Delta$, their upper bounds are, respectively, $f_B(g)+\Delta = 0.5$ and $f_B(g)/(1-\alpha)$, and hence, we have $f_B(g)+\Delta = f_B(g)/(1-\alpha) = 0.5$. Through some manipulation, we have $\Delta = 0.5\alpha$ and then Eq. (8) can further be simplified as a function of α as follows:

$$f_B(g) = \begin{cases} \sqrt{g} & \text{for } 0 \le g \le 0.25(1-\alpha)^2 \\ 0.5(1-\alpha) & \text{for } 0.25(1-\alpha)^2 \le g \le 0.5 \\ f_B(1-g) & \text{for } 0.5 < g \le 1 \end{cases}. \tag{9}$$

Equation (9) shows the desired principal radial frequencies for individual gray levels. By substituting Eq. (9) into Eq. (7), the bounds of $\Phi_B(g)$ are well defined as functions of g and α. According to BNM_2, most of the noise energy should concentrate in frequency band $\Phi_B(g)$. Hence, the optimal diffusion filter for a particular gray level g can be determined by maximizing the noise energy in $\Phi_B(g)$ as follows:

$$\mathbf{w}^{\mathrm{opt}}(g) = \arg\max_{\mathbf{w}} \sum_{(u,v)\in\Phi_B(g)} \hat{P}_{\mathbf{w}}(u,v;g) \tag{10}$$

under constraints

$$\sum_{(k,l)\in L_z} w(k,l) = 1 \quad \text{and} \quad w(k,l) \ge 0 \quad \text{for all } (k,l) \in L_z, \tag{11}$$

where $\mathbf{w}^{\mathrm{opt}}(g)$ is the optimal diffusion filter for gray level g, $w(k,l)$ is the (k,l)'th coefficient of a diffusion filter denoted as $\mathbf{w}$ with filter support L_z, and $\hat{P}_{\mathbf{w}}(u,v;g)$ is the magnitude of the (u,v)'th component of $\hat{\mathbf{P}}_{\mathbf{w}}(g)$, the estimated magnitude spectrum of the halftone of a constant patch of gray level g. $\hat{\mathbf{P}}_w(g)$ is estimated using the averaging periodogram method based on P windowed portions of the halftone produced by error diffusion with error diffusion filter $\mathbf{w}$. In formulation, we have

$$\hat{\mathbf{P}}_{\mathbf{w}}(g) = \frac{1}{P}\sum_{k=1}^{P} |\mathcal{F}(\mathbf{h}_{\mathbf{w}}^k(g))|, \tag{12}$$

where $\mathcal{F}$ is the discrete Fourier transform operator and $\mathbf{h}_{\mathbf{w}}^k(g)$ is the k'th windowed portion of the halftone of a constant patch of gray level g.

4.2 *Optimization Algorithm*

Without loss of generality, we assume that there are totally 256 possible input gray levels between 0 and 1. We optimized their corresponding diffusion filters sequentially starting with the one for $g = 127/255$. After one filter is optimized, the filter for the next lower gray level is optimized until the one for $g = 1/255$ is done. Since there is no quantization error to diffuse when $g = 0$, the diffusion filter for $g = 0$ is theoretically a "do not care." In our algorithm, it is simply made identical to $\mathbf{w}^{\mathrm{opt}}(1/255)$. Due to the symmetry property, diffusion filters for $g \ge 128/255$ can be obtained by $\mathbf{w}^{\mathrm{opt}}(g) = \mathbf{w}^{\mathrm{opt}}(1-g)$.

Theoretically, one can exploit any optimization algorithms, such as genetic algorithm[37] or simulated annealing,[38] to search the optimal diffusion filter for gray level g based on objective function [Eq. (10)] under constraints [Eq. (11)]. We believe that there will not be any major difference in the optimization results. The diffusion filters reported in this paper

Downloaded From: https://www.spiedigitallibrary.org/journals/Journal-of-Electronic-Imaging on 09 Nov 2022
Terms of Use: https://www.spiedigitallibrary.org/terms-of-use

were optimized with the optimization algorithm, the pseudocode of which is given in Fig. 3. According to our simulation results, the set of filters optimized with the algorithm is good enough to provide halftones of the desired noise characteristics specified by BNM_2 and also produce halftones of good quality in real applications.

The optimization algorithm is an iterative algorithm in which a filter is updated iteratively to maximize the objective function. Before it starts, a filter for gray level g, say $\mathbf{w}^*(g)$, is initialized as

$$\mathbf{w}^*(g) = \begin{cases} \mathbf{w}^{\text{opt}}(g+1/255) & \text{if } g < 127/255 \\ \mathbf{w}_0 & \text{if } g = 127/255 \end{cases}, \tag{13}$$

where $\mathbf{w}_0$ is a filter whose coefficients are given as $w_0(k,l) = A/(\sqrt{k^2+l^2})$ for $(k,l) \in L_z$. A is a normalization factor to make $\sum_{(k,l)\in L_z} w_0(k,l) = 1$.

In each iteration i, a new diffusion filter $\mathbf{w}^i(g)$ is generated by randomly perturbing the coefficient values of $\mathbf{w}^*(g)$ under the constraint that $\mathbf{w}^i(g) \in \Omega$, where Ω is defined as

$$\Omega = \Big\{ \mathbf{w} | 1 \geq w(k,l) \geq 0 \quad \text{and} \quad |w(k,l) - w^*(k,l;g)| \leq \varepsilon, \quad \forall\ (k,l) \in L_z \quad \text{and} \quad \sum_{(k,l)\in L_z} w(k,l) = 1 \Big\}. \tag{14}$$

In Eq. (14), $w(k,l)$ and $w^*(k,l;g)$ are, respectively, the (k,l)'th coefficients of filters $\mathbf{w}$ and $\mathbf{w}^*(g)$, and ε is a parameter that controls the maximum amount of perturbance.

After generating filter $\mathbf{w}^i(g)$, $\mathbf{w}^*(g)$is conditionally updated as follows.

$$\mathbf{w}^*(g) = \mathbf{w}^i(g) \quad \text{if} \sum_{(u,v)\in\Phi_B(g)} \hat{P}_{\mathbf{w}^i(g)}(u,v;g) > \sum_{(u,v)\in\Phi_B(g)} \hat{P}_{\mathbf{w}*(g)}(u,v;g). \tag{15}$$

In other words, we keep the filter that can produce an halftone that contains more noise energy in frequency band $\Phi_B(g)$. This guarantees that $\mathbf{w}^*(g)$ is the best diffusion filter in all the candidates and we tested so far. As parameter ε is decreased every N iterations, the size of set Ω shrinks and hence, the convergence of $\mathbf{w}^*(g)$ is guaranteed. The final $\mathbf{w}^*(g)$ is selected as $\mathbf{w}^{\text{opt}}(g)$.

```
Select filter support L_z
Set iteration bound N=100
Set perturbance bound ε_0=0.025
Initialize diffusion filter w*(g) with eqn. (13)
For β=1:-0.2:0.2
    ε = ε_0 ×β
    For iteration i=1:N
        Perturb w*(g) to get w^i(g) ∈ Ω
        Update w*(g) with eqn. (15)
    End
End
w^opt(g) = w*(g)
```

Fig. 3 The pseudocode for optimizing a diffusion filter for gray level g.

4.3 *Selection of L_z and α*

To reduce the complexity of the optimization, it would be better to confine the size of diffusion filter $\mathbf{w}^{\text{opt}}(g)$ before optimizing it. By considering that a larger diffusion filter incurs a higher realization complexity and tends to blur the local spatial details in the resultant halftone images, we limit our choices to a few sizes purposely. Figure 4 shows four templates that define the support windows of the filters we investigated in our study. Template L_4 has the minimum size and it covers 4 pixels. Templates L_6, L_{10}, and L_{12} are obtained by gradually expanding L_4. It is achieved by gradually including the next nearest neighbors of *. Though these filters are small, our simulation results shown in later sections can prove that after optimization, they are already good enough to produce halftones of the desired noise characteristics.

Parameter α is a crucial parameter for the optimization of the diffusion filters because, as shown in Eq. (7), it determines the bandwidth of $\Phi_B(g)$ on which the objective function is based. Since the diffusion filters are optimized to maximize the noise energy of a halftone in $\Phi_B(g)$, one can expect that the noise energy peak falls in $\Phi_B(g)$. In other words, parameter α actually controls the principal radial frequency $f_B(g)$ of the expected halftoning results obtained with the optimized filters.

As shown in Eq. (9), the target principal radial frequency $f_B(g)$ is bounded by $0.5(1-\alpha)$ when $1-0.25(1-\alpha)^2 \geq g \geq 0.25(1-\alpha)^2$. This can only be achieved by clustering dots and then maintaining an average distance of $2/(1-\alpha)$ between the centers of two neighboring dot clusters. The larger the value of α, the more the extent of clustering is required. However, conceptually, it is more difficult to preserve the fine spatial details with larger dot clusters. In view of this factor, we should minimize α to make $f_B(g)$ as close to 0.5 as possible under the constraint that α is large enough to make $\Phi_B(g)$ practically possible to accommodate most of the noise energy of a halftone.

Figure 5 shows the impacts of α on the achieved noise characteristics of the halftones obtained with the diffusion filters optimized with the proposed optimization algorithm. The results were optimized under the condition that the filter support is L_6. The achieved noise characteristics are presented as plots of radially averaged power spectrum density (RAPSD). RAPSD is a measure proposed in Ref. 9 for

		*	$w_{0,1}$	$w_{0,2}$
$w_{1,-2}$	$w_{1,-1}$	$w_{1,0}$	$w_{1,1}$	$w_{1,2}$
$w_{2,-2}$	$w_{2,-1}$	$w_{2,0}$	$w_{2,1}$	$w_{2,2}$

(a) Support L_{12}

		*	$w_{0,1}$	$w_{0,2}$
$w_{1,-2}$	$w_{1,-1}$	$w_{1,0}$	$w_{1,1}$	$w_{1,2}$
	$w_{2,-1}$	$w_{2,0}$	$w_{2,1}$	

(b) Support L_{10}

		*	$w_{0,1}$	$w_{0,2}$
	$w_{1,-1}$	$w_{1,0}$	$w_{1,1}$	
		$w_{2,0}$		

(c) Support L_6

		*	$w_{0,1}$	
	$w_{1,-1}$	$w_{1,0}$	$w_{1,1}$	

(d) Support L_4

Fig. 4 Four templates of filter supports. (a) Support L_{12}, (b) Support L_{10}, (c) Support L_6, and (d) Support L_4.

Downloaded From: https://www.spiedigitallibrary.org/journals/Journal-of-Electronic-Imaging on 09 Nov 2022
Terms of Use: https://www.spiedigitallibrary.org/terms-of-use

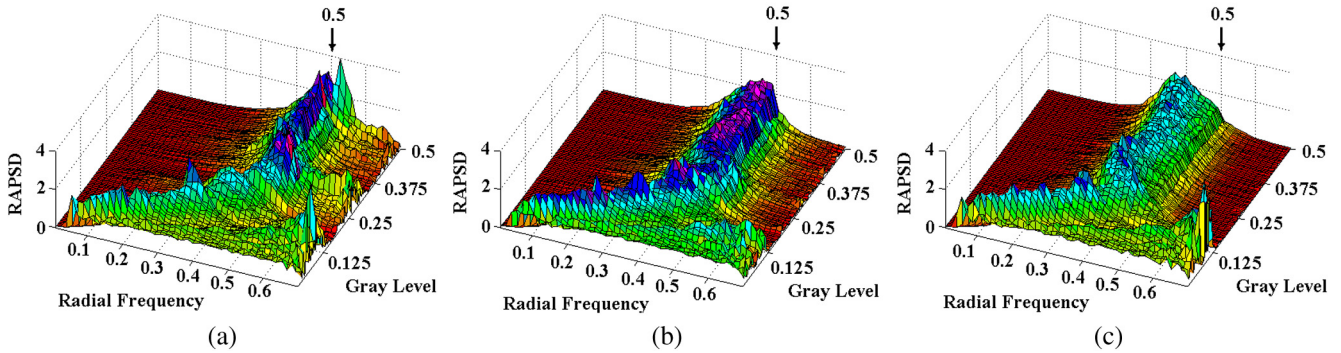

Fig. 5 The RAPSD plots for $\alpha =$ (a) 0.02, (b) 0.1, and (c) 0.2 when diffusion filters with support template L_6 are used.

analyzing the spectral characteristics of a halftone pattern. The ridges in the plots mark the principal radial frequencies of particular gray levels in their halftoning results.

One can see in Fig. 5 that a larger α shifts the principal radial frequencies more away from 0.5 when $g > 0.25$. The amount of shift is roughly $0.5(1-\alpha)$ as specified in Eq. (9). This verifies that by tuning parameter α of the objective function, one can effectively control the noise characteristics of the halftones obtained with the optimized set of diffusion filters.

As shown in Fig. 5(a), when $\alpha = 0.02$, the principal radial frequencies are very close to 0.5. The energy peak tails extend into Φ_z, the region in which the radial frequencies are >0.5. This corresponds to the case shown in Fig. 2(c). Accordingly, aliasing problem exists and pattern noise is expected in the halftoning results. This finding is not a surprise as BNM_1 can be considered as a special case of BNM_2 where $\alpha = 0$.

Another observation we have is that, as shown in Figs. 5(b) and 5(c), the amount of energy in Φ_z is more or less the same in cases when $\alpha = 0.1$ and 0.2. It implies that the extent of clustering is unnecessarily increased in the cases when $\alpha > 0.1$. Based on this observation, $\alpha = 0.1$ is suggested in this paper. All later discussions are mainly based on the optimization results obtained with $\alpha = 0.1$ unless other values are specified.

Let us recall that our proposed diffusion filters are optimized by maximizing objective function:

$$J = \sum_{(u,v)\in\Phi_B(g)} \hat{P}_{\mathbf{w}}(u,v;g). \tag{16}$$

For each filter support window L_z and gray level g, a corresponding optimized filter $\mathbf{w}^{\text{opt}}(g)$ can be obtained with the optimization algorithm given in Fig. 3. Figure 6 shows the performance achieved by the $\mathbf{w}^{\text{opt}}(g)$ optimized for a specific combination of L_z and g in terms of J value. One can see that, when $0.5 \geq g \geq 0.16$, there is no major performance difference among the filters with support windows L_6, L_{10}, and L_{12} while the filters with support window L_4 have a lower performance than the others. When $0 \leq g < 0.16$, in most of the cases, the filters with support window L_4 are better than those with support window L_6, and their performance is comparable with that of the filters with support windows L_{10} and L_{12}. Since a larger diffusion filter implies more realization effort in error diffusion, we use optimized filters with support window L_4 for $0 \leq g < 0.16$ and optimized filters with support window L_6 for $0.5 \geq g \geq 0.16$ to reduce the complexity of the proposed TDED algorithm.

Apparently, this arrangement causes discontinuity at $g = 0.16$ and may introduce visual discontinuity in the halftoning output around $g = 0.16$. However, this problem does not happen in our simulation results. Note that filters for different gray levels are independently trained according to the model to provide the desirable noise characteristics. As long as the filters around $g = 0.16$ are well trained to provide halftoning outputs of the same characteristics, their outputs can mix harmoniously without discontinuity artifacts.

Figure 7 shows the coefficient values of the $\mathbf{w}^{\text{opt}}(g)$ used in our proposed TDED algorithm for $0.5 \geq g \geq 0$. Though $\mathbf{w}^{\text{opt}}(g)$ for $g < 0.16$ are actually filters with support window L_4, in Fig. 7, they are presented as filters with support window L_6 coefficients $w(2,0)$ and $w(0,2)$ of which are both 0. Diffusion filters for $1 \geq g \geq 0.5$ can be obtained by $\mathbf{w}^{\text{opt}}(g) = \mathbf{w}^{\text{opt}}(1-g)$.

4.4 *Use of the Filters*

The proposed TDED algorithm scans an input image with serpentine scanning and processes the pixels sequentially. For each pixel, it quantizes its accumulated pixel value and then diffuses the quantization error with filter $\mathbf{w}^{\text{opt}}(g')$, where g' is the original intensity value of the pixel. When the quantization threshold is fixed to be 0.5, this algorithm is referred to as TDED_B. The subscript B indicates that the

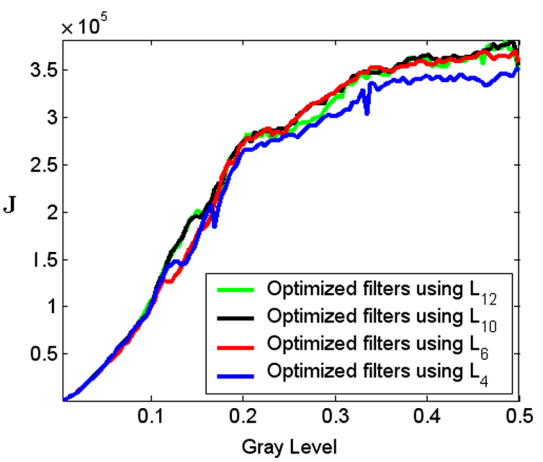

Fig. 6 The J performance of different optimized filters.

Downloaded From: https://www.spiedigitallibrary.org/journals/Journal-of-Electronic-Imaging on 09 Nov 2022
Terms of Use: https://www.spiedigitallibrary.org/terms-of-use

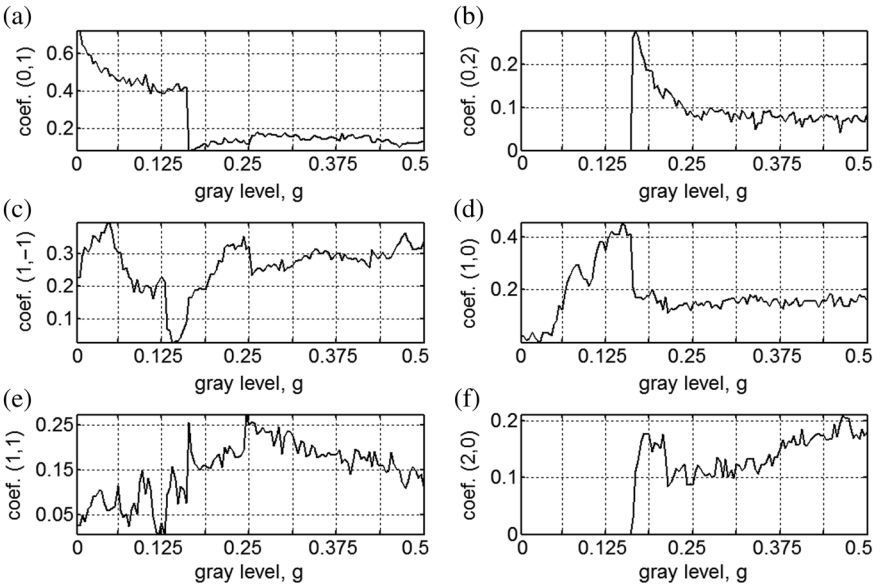

Fig. 7 The coefficient values of the optimized diffusion filters for $0 \le g \le 0.5$. (a) Coef. (0,1) versus gray level, g, (b) Coef. (0,2) versus gray level, g, (c) Coef. (1, −1) versus gray level, g, (d) Coef. (1,0) versus gray level, g, (e) Coef. (1,1) versus gray level, g, and (f) Coef. (2,0) versus gray level, g.

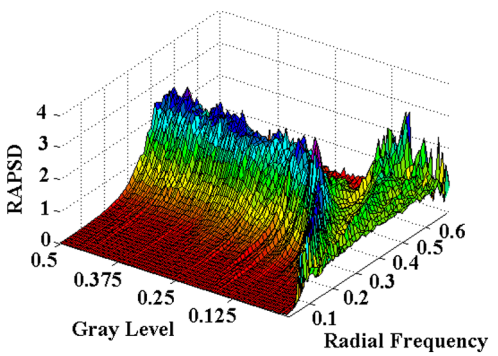

Fig. 8 The RAPSD plot of $TDED_B$.

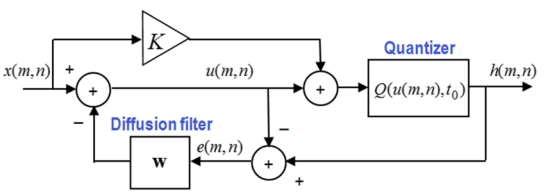

Fig. 9 Modified error diffusion.

TDED algorithm is optimized based on the blue noise model presented in Ref. 36. Figure 8 shows the RAPSD performance of $TDED_B$. Up to this point, the proposed TDED algorithm has not yet taken the sharpening effect of a diffusion filter into account. In Sec. 5, this issue will be addressed and the proposed TDED algorithm will be further improved.

5 Optimization of Thresholds

Sharpening is an inherent property of the conventional error diffusion system shown in Fig. 1 and its extent is diffusion filter dependent. Knox and Eschbach[18] introduced a modification to the error diffusion system shown in Fig. 1 by adding a feed-forward path, as shown in Fig. 9, to directly control the extent of sharpening with the path gain K. It provides us a means to compensate for the sharpening effect as long as we can measure the extent of the sharpening introduced by the original error diffusion system.

Kite et al.[19] show that the sharpening effect of the error diffusion system shown in Fig. 1 can be reflected by the linear signal gain of its quantizer. This linear signal gain, denoted as K_s here, can be evaluated by analyzing the system under the conditions that (1) the input image is normalized such that its original intensity values are bounded in [−0.5, 0.5], (2) the quantizer threshold is 0, and (3) the quantizer output is either −0.5 or 0.5. In formulation, it is defined as

$$K_s = \frac{\sum_{i,j} x'(i,j)y(i,j)}{\sum_{i,j} x'(i,j)^2}, \tag{17}$$

where $x'(i,j)$ is the input to the quantizer for pixel (i,j) and $y(i,j)$ is its output.

For a system whose input pixel value and quantizer threshold are, respectively, $g \in [0,1]$ and $t_0 = 0.5$ as assumed in our discussion, the requested conditions for the system analysis can be satisfied after offsetting the system's input, threshold and output values by −0.5.

According to the linear gain model of Kite et al.,[19] sharpening or blurring is introduced by the error diffusion algorithm when $K_s \neq 1$. If one wants to compensate for the sharpening effect by modifying the system, as shown in Fig. 9, then the forward path gain K should be adjusted to be

$$K = (1 - K_s)/K_s. \tag{18}$$

Note that Eq. (18) is only valid for a system whose input is bounded in [−0.5, 0.5] and whose threshold is 0 as K_s is estimated under the aforementioned conditions.

Downloaded From: https://www.spiedigitallibrary.org/journals/Journal-of-Electronic-Imaging on 09 Nov 2022
Terms of Use: https://www.spiedigitallibrary.org/terms-of-use

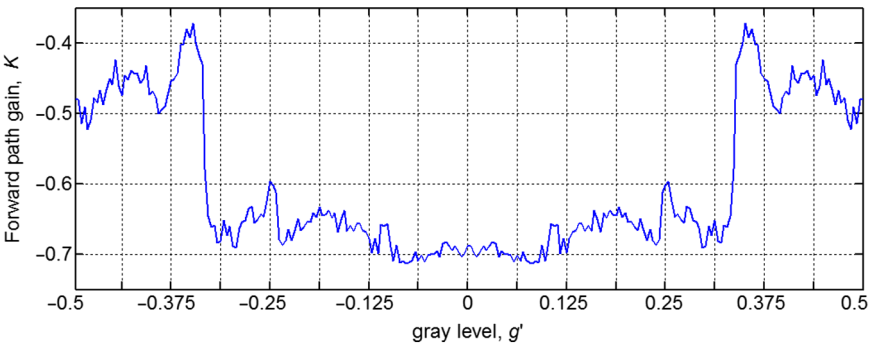

Fig. 10 Gray level dependent forward path gain for input gray level $x(m,n) = g' \in [-0.5, 0.5]$.

The proposed TDED_B basically adopts the same system framework shown in Fig. 1, so its sharpening compensation can also be carried out based on a similar analysis after some modifications. In TDED_B, a particular diffusion filter $\mathbf{w}^{\text{opt}}(g)$ for $g \in [0,1]$ can only be used for a particular input gray level g, which makes K g-dependent as K is diffusion filter dependent. To study the sharpening effect introduced by a specific $\mathbf{w}^{\text{opt}}(g)$ in the system setup shown in Fig. 1, we evaluated the corresponding linear signal gain K_s with a 512×512 constant patch of gray level $g' = g - 0.5 \in [-0.5, 0.5]$ as the input image after offsetting the system's threshold and output values as mentioned earlier. After evaluating one K_s for each diffusion filter used in TDED_B, the one-to-one correspondence between $\mathbf{w}^{\text{opt}}(g)$ and g' allows us to have a K_s value for each input gray level g'. The corresponding K value for each input gray level can then be obtained with formulation [Eq. (18)] and their connection is shown in Fig. 10. As K is g'-dependent, it can be considered as a function of g' and the K value for gray level g' is denoted as $K(g')$ hereafter.

The change of $K(g')$ at $g' = \pm 0.34$ corresponds to the change between support windows L_4 and L_6 at $g = 0.16$ and 0.84. At a first glance, one may think that this dramatic change may introduce un-natural boundary effect in a halftoning output. In fact, $K(g')$ is only an intermediate parameter for deriving the tone-dependent threshold used in the compensation. We will see that the dramatic change in $K(g')$ does not cause a dramatic change in the threshold and hence, we need not overly worry about it at this early stage.

With the obtained tone-dependent K on hand, the sharpening effect of TDED_B can be compensated by adopting the system framework shown in Fig. 9 and making the forward path gain be $K(x(m,n))$, where $x(m,n) \in [-0.5, 0.5]$ is the original intensity value of the pixel being processed.

Adding a feed-forward path to the original error diffusion system, as shown in Fig. 9, is actually equivalent to turning the quantizer threshold of the system shown in Fig. 1 from constant t_0 into a function of $x(m,n)$ as

$$t_0' = t_0 - K[x(m,n)) \cdot (x(m,n)]. \tag{19}$$

The quantizer threshold then becomes tone dependent. When $x(m,n) \in [0,1]$ instead of $[-0.5, 0.5]$ and the original threshold t_0 is 0.5 as assumed in our earlier discussion, the quantizer threshold should be adjusted to

$$t_0' = 0.5 - K(x(m,n) - 0.5) \cdot (x(m,n) - 0.5). \tag{20}$$

Figure 11 shows how t_0' should change with $x(m,n)$ when $x(m,n) \in [0,1]$. As mentioned before, there is no dramatic change at $g = 0.16$ and 0.84.

In summary, the proposed TDED_B can be further improved to compensate for the sharpening effect introduced by the diffusion filters by just replacing the original quantizer threshold 0.5 with a tone-dependent quantizer threshold. This improved algorithm adjusts its quantizer threshold and error diffusion filter according to the original input intensity value of the pixel being processed. For reference purpose, this improved algorithm is referred to as TDED_BS hereafter. The subscript S indicates that there is a sharpening control in the improved algorithm.

6 Performance Analysis

An analysis was carried out to study the performance of TDED_BS and the results are reported in this section. For comparison, the performance of some conventional error diffusion algorithms, including Floyd and Steinberg,[3] Jarvis

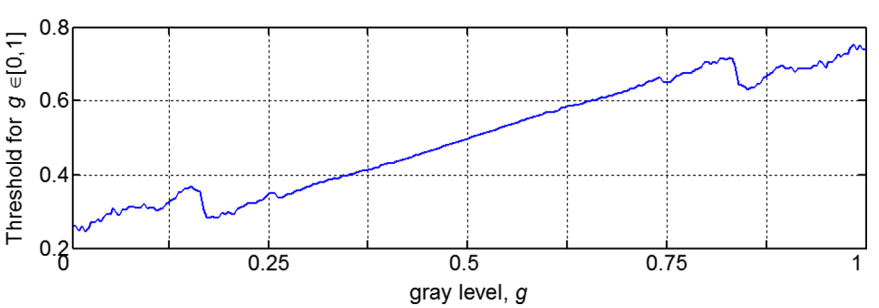

Fig. 11 Tone-dependent threshold for $x(m,n) = g \in [0,1]$.

Downloaded From: https://www.spiedigitallibrary.org/journals/Journal-of-Electronic-Imaging on 09 Nov 2022
Terms of Use: https://www.spiedigitallibrary.org/terms-of-use

and Roberts,[4] Ostromoukhov,[31] Li and Allebach,[32] Hwang et al.,[33] and Zhou and Fang,[34] was also evaluated. Among them, Ostromoukhov,[31] Hwang et al.,[33] and Zhou and Fang[34] are optimized according to BNM. The algorithm in Ref. 32 is not optimized based on any discussed blue noise models, but it is well believed to be one of the best halftoning algorithms. There are several versions of the algorithm presented in Ref. 32. In our simulation, the one that works with two-row serpentine scan was implemented for comparison as it provides the best performance in removing artifacts. As there is no reported error diffusion algorithm developed based on BNM_1, no algorithm in this category is involved in our comparison study. Last, we note that Ostromoukhov,[31] Li and Allebach,[32] Hwang et al.,[33] and Zhou and Fang[34] are all TDED algorithms as the proposed algorithm does. For each input gray level, they exploit a corresponding optimized filter to carry out the error diffusion.

In our study, constant gray level patches of size 512×512 were halftoned with different evaluated algorithms. To avoid startup delay, five additional rows of random numbers are packed at the top of the patches and only the central portions of the halftoning outputs were used for analysis.

Some input gray levels, such as 1/255, 64/255, 85/255, and 127/255, are potentially problematic for error diffusion algorithms. Figure 12 shows the central portions of the halftoning results of these gray levels. One can see that the proposed $TDED_{BS}$ and Zhou et al.'s algorithm can successfully eliminate the directional artifacts and regular structure patterns while the others cannot when handling these problematic levels.

Figure 13 shows the spectra of the halftones that are partially shown in Fig. 12. For better comparison, all spectra for the same input gray level g are normalized with respect to the maximum magnitude value of all their frequency components. One can see that the strong frequency components around the principal radial frequencies form perfect circular bands in the spectra of the proposed $TDED_{BS}$ for all gray levels. It proves that the noise characteristics of $TDED_{BS}$'s halftoning outputs comply with BNM_2. By contrast, bright spots or irregular patterns can be found in the spectra of other evaluated algorithms except the algorithm of Zhou and Fang[34] for some evaluated gray levels. These spots and patterns explain why there are patterns and directional artifacts in the corresponding halftones shown in Fig. 12.

Figures 12 and 13 only show the results of some input gray levels. To have a complete picture, constant patches of all 8-bit gray levels were halftoned with different error diffusion algorithms and their outputs were evaluated in terms of RAPSD and anisotropy. RAPSD and anisotropy are two measures commonly used to analyze the spectral characteristics of a halftone pattern. The details of their definitions can be found in Ref. 16.

Figure 14 shows the RAPSD plots of various algorithms. In these plots, all RAPSD values are clipped by 4 such that an easier comparison can be made among the plots. Among the evaluated algorithms, algorithms of Floyd and Steinberg,[3] Jarvis and Roberts,[4] and Li and Allebach[32] are not purposely designed to comply with any noise models. For some specific gray levels, there are outstanding peaks at some radial frequencies other than the principal radial frequencies in the RAPSD plots of algorithms.[3,4] These peaks contribute severe pattern artifacts in the halftones of these levels.

Algorithms[31,33] are optimized for BNM. One can see that there are still some occasional isolated energy peaks in their RAPSD plots. Besides, when $g \in [0.25, 0.75]$, energy is packed in a range of radial frequencies instead of one single

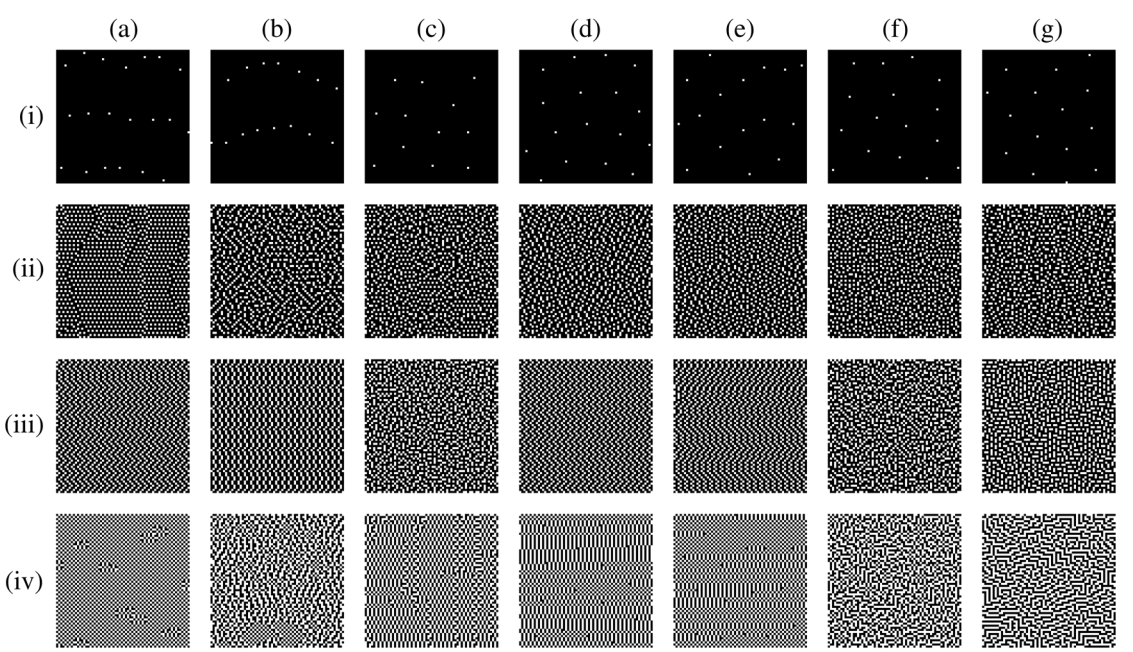

Fig. 12 The central portions of halftones of various algorithms. From left to right: (a) Floyd and Steinberg,[3] (b) Jarvis and Roberts,[4] (c) Li and Allebach,[32] (d) Ostromoukhov,[31] (e) Hwang et al.,[33] (f) Zhou and Fang,[34] and (g) $TDED_{BS}$. From top to bottom: (i) $g = 1/255$, (ii) $g = 64/255$, (iii) $g = 85/255$, and (iv) $g = 127/255$.

Downloaded From: https://www.spiedigitallibrary.org/journals/Journal-of-Electronic-Imaging on 09 Nov 2022
Terms of Use: https://www.spiedigitallibrary.org/terms-of-use

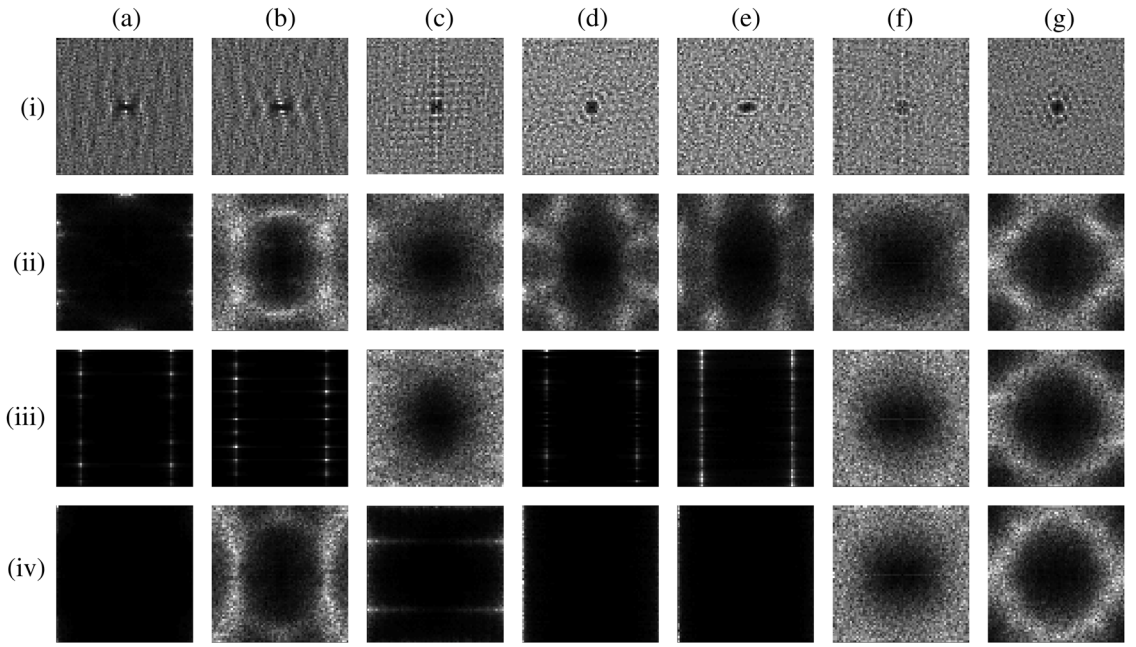

Fig. 13 The corresponding spectra of Fig. 12. From left to right: (a) Floyd and Steinberg,[3] (b) Jarvis and Roberts,[4] (c) Li and Allebach,[32] (d) Ostromoukhov,[31] (e) Hwang et al.,[33] (f) Zhou and Fang,[34] and (g) TDED_{BS}. From top to bottom: (i) $g = 1/255$, (ii) $g = 64/255$, (iii) $g = 85/255$, and (iv) $g = 127/255$.

principal radial frequency in their RAPSD plots. Figure 2(b) serves as a good hint to explain this phenomenon. When $g \in [0.25, 0.75]$, the aliasing of $B(f_B(g))$ maintains a wide band of strong components in the high radial frequency region.

Algorithm[32] is not optimized for any discussed blue noise models, but its RAPSD plot is similar to those of algorithms[31,33] in a way that energy is also packed in a range of radial frequencies when $g \in [0.25, 0.75]$ and the lower bound of the range is around radial frequency 0.5.

Figure 14(g) shows the RAPSD plot of the proposed TDED_{BS}. One can see that the noise spectral characteristics of TDED_{BS} successfully comply with BNM_2 [Eq. (9)]. There is only one single energy peak at the target principal radial frequency when $g \in [0.25, 0.75]$. Note that this can only be achieved when the noise spectra of the halftoning results of all these gray levels are isotropic. Accordingly, one can expect that there is no pattern and directional artifact.

Although algorithm[34] is claimed to be optimized for BNM, its RAPSD shows that its noise characteristics is actually biased to model BNM_2 instead of BNM. One can see that its RAPSD is very similar to TDED_{BS}'s. It explains why the quality of its halftoning outputs is better than those of algorithms.[3,4,31–33]

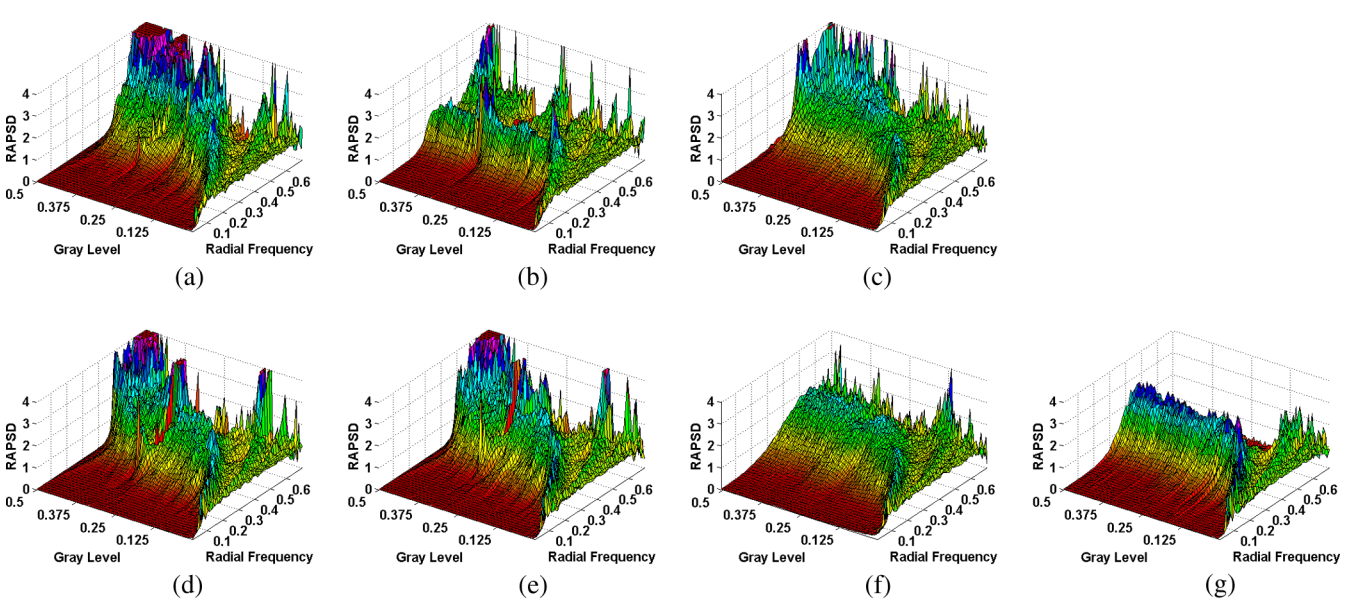

Fig. 14 The RAPSD plots of various algorithms: (a) Floyd and Steinberg,[3] (b) Jarvis and Roberts,[4] (c) Li and Allebach,[32] (d) Ostromoukhov,[31] (e) Hwang et al.,[33] (f) Zhou and Fang,[34] and (g) TDED_{BS}.

Downloaded From: https://www.spiedigitallibrary.org/journals/Journal-of-Electronic-Imaging on 09 Nov 2022
Terms of Use: https://www.spiedigitallibrary.org/terms-of-use

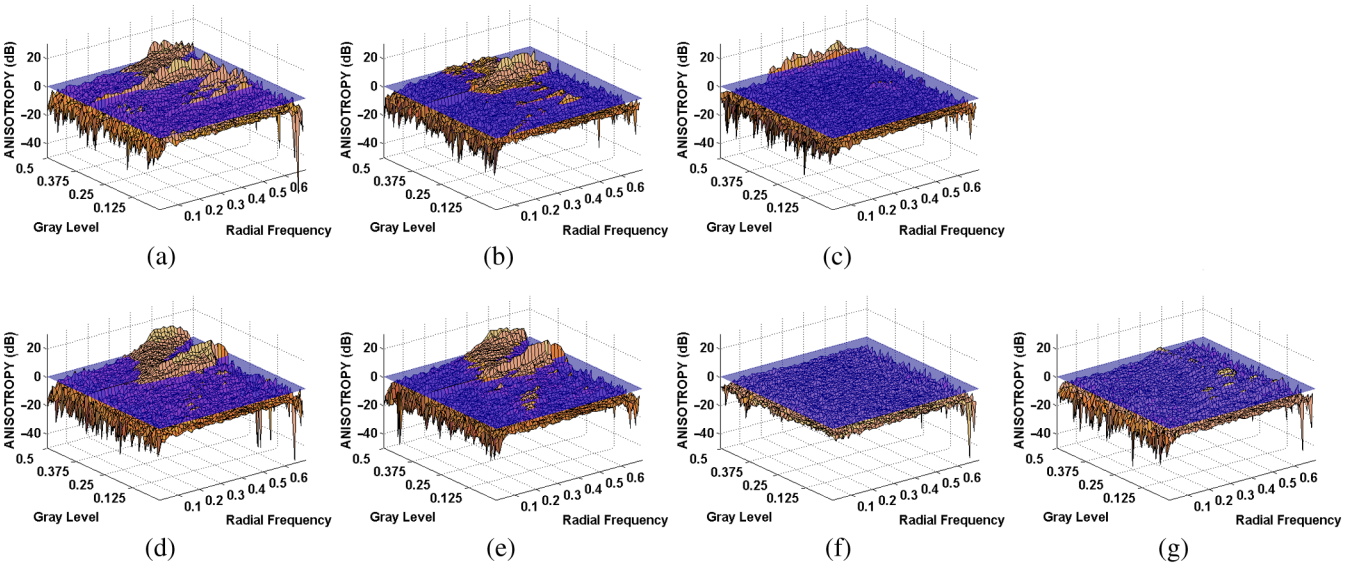

Fig. 15 The anisotropy plots of various algorithms: (a) Floyd and Steinberg,[3] (b) Jarvis and Roberts,[4] (c) Li and Allebach,[32] (d) Ostromoukhov,[31] (e) Hwang et al.,[33] (f) Zhou and Fang,[34] and (g) TDED_{BS}.

Figure 15 shows the anisotropy plots of various algorithms. Anisotropy measures the strength of directional artifacts and it is well accepted that directional artifacts at radial frequency f_r are not visually noticeable when $A(f_r) < 0$ dB happens. One can see that TDED_{BS} and Zhou et al.'s algorithm are obviously superior to others in terms of anisotropy. In Figs. 15(f) and 15(g), $A(f_r)$ is below 0 dB for almost all radial frequencies and all gray levels. For other algorithms except Li and Allebach,[32] their anisotropy performance is generally good for gray levels from 0 to 0.25 only. These algorithms were not developed based on BNM_2 and hence, as shown in Fig. 2, there will be aliasing problem for $g \in [0.25, 0.75]$ even though some of them are optimized according to BNM. In consequence, visible directional artifacts are expected in their outputs when $g \in [0.25, 0.75]$. By contrast, the noise spectra associated with TDED_{BS} are all close to isotropic as requested by BNM_2 when $g \in [0.25, 0.75]$. Little directional artifact exists in the halftoning outputs of all gray levels and hence TDED_{BS}'s performance is good in terms of anisotropy. Zhou et al.'s algorithm also has a good performance in terms of anisotropy as it is explicitly optimized to maintain the symmetry of the noise spectrum of its halftoning outputs.

A study was carried out to evaluate the performance of various algorithms in sharpening control as follows. Two 512×256 constant patches of different gray levels are concatenated to form a 512×512 step image and then processed to produce halftones with different algorithms. For each halftone, pixel values of each column are averaged and the average value of a column is plotted against the displacement of the column from the edge to describe the step response of the corresponding algorithm for comparison. Figure 16 shows the responses of different algorithms when the two gray levels are 0.3 and 0.7. One can see that with our matched tone-dependent sharpening compensation method, the overshoot at the edge in TDED_{B}'s response can be eliminated in TDED_{BS}'s response. In terms of the overshoot extent, algorithm[32] also performs well in sharpening control. In fact,

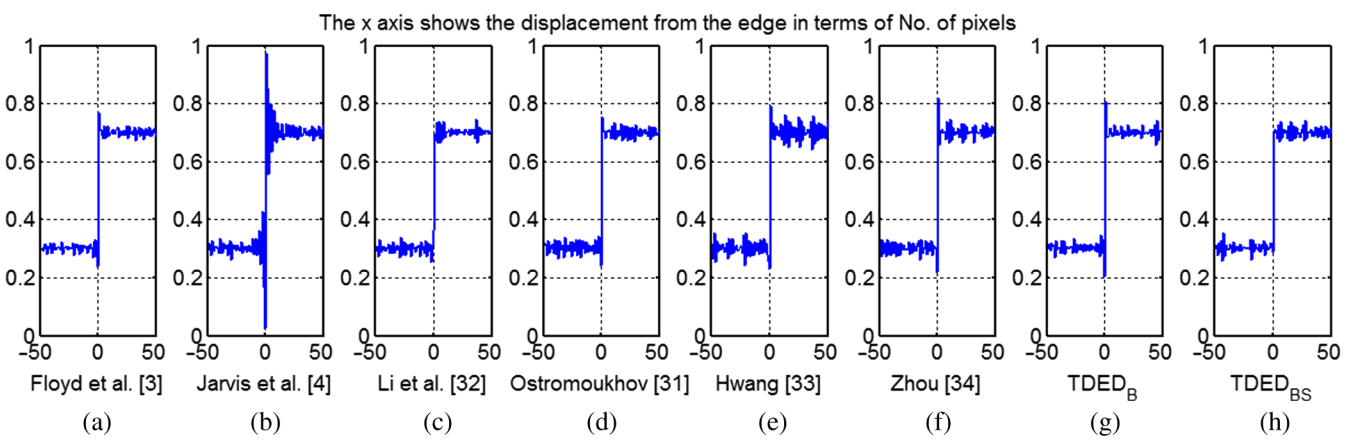

Fig. 16 Step responses of various algorithms. (a) Floyd and Steinberg,[3] (b) Jarvis and Roberts,[4] (c) Li and Allebach,[32] (d) Ostromoukhov,[31] (e) Hwang et al.,[33] (f) Zhou and Fang,[34] (g) TDED_{B}, and (h) TDED_{BS}.

Downloaded From: https://www.spiedigitallibrary.org/journals/Journal-of-Electronic-Imaging on 09 Nov 2022
Terms of Use: https://www.spiedigitallibrary.org/terms-of-use

among all evaluated algorithms, only $TDED_{BS}$ and Li and Allebach[32] take the sharpening issue into account and resolve it proactively. Similar results can be obtained when other gray levels were used to construct the step image.

7 Simulation Results

To study the performance of the evaluated algorithms on real images, some 8-bit gray level testing images of size 512×512 are halftoned with these algorithms separately. The testing images include "mandrill," "Barbara," "boat," "fruits," "house," "Lena," "man," "peppers," "airplane," and "girl" in our simulations.

Figures 17 and 18 show some simulation results for comparison. Their ground truth is shown in Fig. 19. Specifically, Fig. 17 shows portions of different halftoning results of testing image "fruits." Directional artifacts and regular structure patterns can be found in the halftones produced by Floyd and Steinberg,[3] Jarvis and Roberts,[4] Ostromoukhov,[31] Li and Allebach,[32] and Hwang et al.[33] while there are no such artifacts in the outputs of the proposed $TDED_B$ and $TDED_{BS}$. Figure 17(b) is obviously sharper than the other results shown in Fig. 17 due to the sharpening effect of the diffusion filter used in algorithm.[4] As compared with Fig. 17(h), Fig. 17(g) is a bit sharper as no compensation for sharpening is carried out in $TDED_B$. The sharpness of Figs. 17(c) and 17(h) is more or less the same. Among the evaluated algorithms, only $TDED_{BS}$ and Li and Allebach[32] take the sharpening effect of diffusion filters into account and perform corresponding sharpening compensation accordingly. Their results can hence truly reflect the sharpness of the original image in terms of K_s.

Figure 18 shows the results for testing image "Lena." The same observations mentioned above can be made. In fact, the mixtures of directional artifacts and regular structure patterns are even more visible in the background regions in Figs. 18(a)–18(e). They form noticeable false contouring artifacts that are visually disturbing. By contrast, the outputs of $TDED_{BS}$ show no such false contouring artifacts and can present a smoothly changing background as in the original. As for Fig. 18(f), broken pieces of checkerboard pattern can be found in its upper portion.

Figure 20 shows the halftoning results of a ramp image. Regular structure patterns can be easily found in Figs. 20(a), 20(b), 20(d), and 20(e). Figure 20(c) contains some regular structure patterns in the midtone region, whereas Fig. 20(g) does not. One can see that there is a smooth transition around $g = 0.84$ in Fig. 20(g). The switch between filter supports L_4 and L_6 does not introduce un-natural boundary effect in a halftoning output.

Since clusters instead of dots are introduced by $TDED_{BS}$ when handling the midtone gray levels, worm patterns are visible in Fig. 20(g) when the input gray level is close to 0.5. However, as mentioned in Ref. 35, worm patterns are not necessarily bad as long as they are not directional and form twisting and turning paths to create a smooth texture. As shown in Figs. 17(f) and 18(f), Zhou et al.'s results do not show worm patterns, but they look noisier than Figs. 17(h) and 18(h) in the smooth regions.

As a final remark, we note that, like the proposed $TDED_{BS}$, both Ostromoukhov[31] and Hwang et al.[33] are TDED algorithms and Hwang et al.[33] optimizes a filter for each gray level as well. However, as shown in Figs. 14(d),

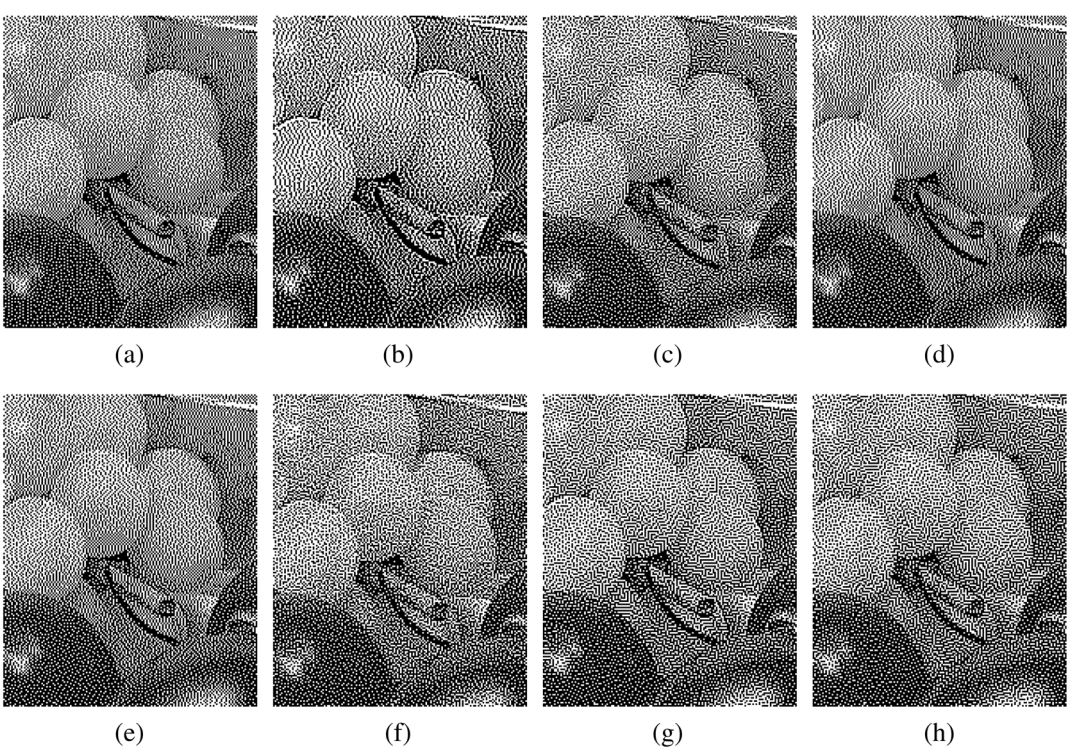

Fig. 17 Portions of halftones of testing image "fruits" generated by various algorithms: (a) Floyd and Steinberg,[3] (b) Jarvis and Roberts,[4] (c) Li and Allebach,[32] (d) Ostromoukhov,[31] (e) Hwang et al.,[33] (f) Zhou and Fang,[34] (g) $TDED_B$, and (h) $TDED_{BS}$.

Downloaded From: https://www.spiedigitallibrary.org/journals/Journal-of-Electronic-Imaging on 09 Nov 2022
Terms of Use: https://www.spiedigitallibrary.org/terms-of-use

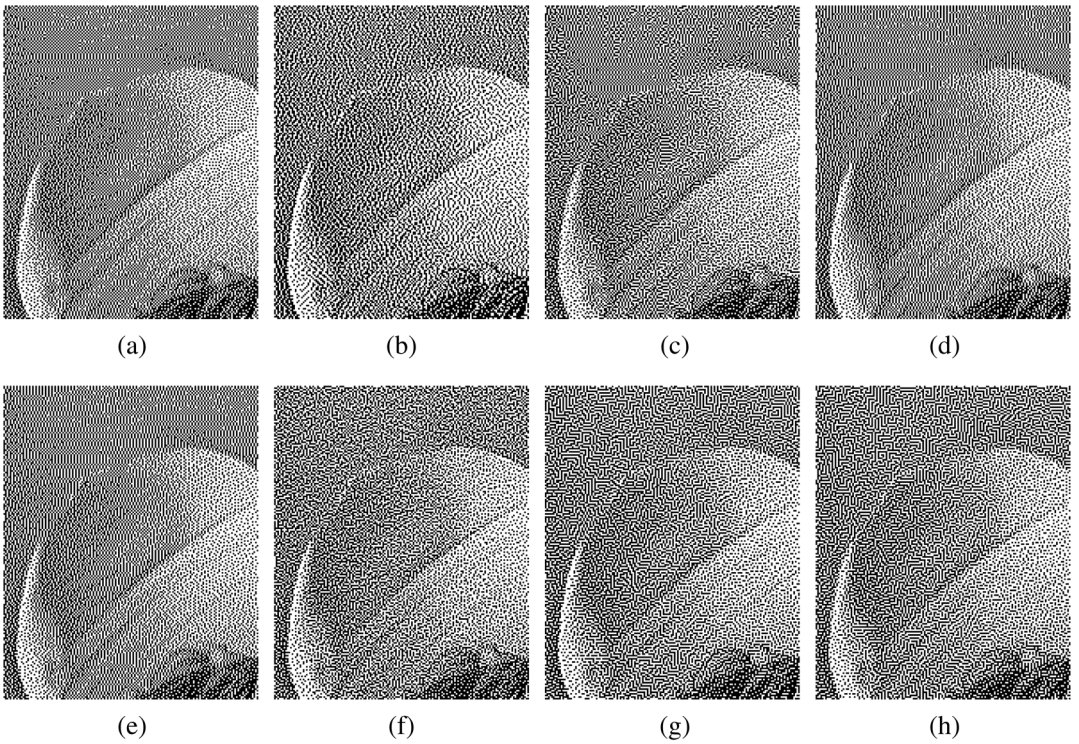

Fig. 18 Portions of halftones of testing image "Lena" generated by various algorithms: (a) Floyd and Steinberg,[3] (b) Jarvis and Roberts,[4] (c) Li and Allebach,[32] (d) Ostromoukhov,[31] (e) Hwang et al.,[33] (f) Zhou and Fang,[34] (g) $TDED_B$, and (h) $TDED_{BS}$.

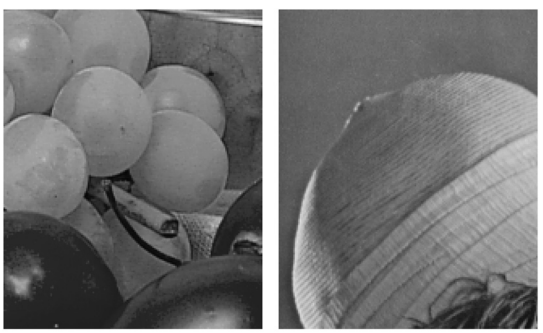

Fig. 19 The ground truth of (a) Fig. 17 and (b) Fig. 18.

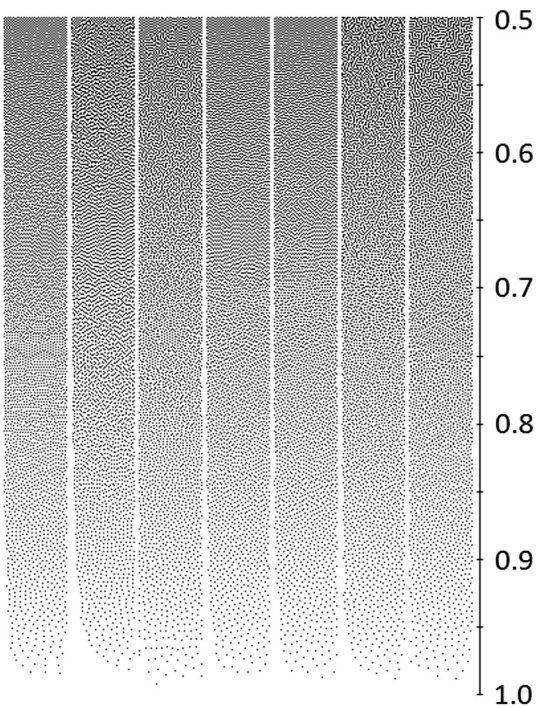

Fig. 20 Ramp images generated by various algorithms: (a) Floyd and Steinberg,[3] (b) Jarvis and Roberts,[4] (c) Li and Allebach,[32] (d) Ostromoukhov,[31] (e) Hwang et al.,[33] (f) Zhou and Fang,[34] and (g) $TDED_{BS}$.

14(e), 15(d), 15(e), 17(d), 17(e), 18(d), 18(e), 20(d), and 20(e), they are still not able to handle some gray levels well. By considering that one of the major differences between $TDED_{BS}$ and them is the target noise model on which their optimization is based, we may deduce that, as compared with BNM, BNM_2 is a better noise model to describe the desirable noise characteristics of a digital haftone in which dots can only be put on grid points. The facts that Zhou et al.'s algorithm[34] can produce halftones of better quality as compared with algorithms[31,33] and that the noise characteristics of its halftones actually fits more to BNM_2 than to BNM also support this interpretation.

8 Conclusions

Error diffusion can produce halftones of fairly good overall quality with little computational complexity such that real-time halftone generation can be supported. In this paper, we proposed a TDED algorithm to produce halftones with the desired noise characteristics specified by the noise model presented in Ref. 36. The algorithm adapts the diffusion filter and the quantizer threshold based on the input intensity value

Downloaded From: https://www.spiedigitallibrary.org/journals/Journal-of-Electronic-Imaging on 09 Nov 2022
Terms of Use: https://www.spiedigitallibrary.org/terms-of-use

of a pixel to produce a halftone. The former adaptation is for producing halftones of the desired noise characteristics while the latter adaptation is for removing the sharpening effect of a typical diffusion filter.

To support the TDED algorithm, we defined a tone-dependent objective function based on the noise model proposed in Ref. 36 and then optimized a diffusion filter for each possible input gray level with the objective function. By bearing the desired noise characteristics, the halftoning outputs of the proposed TDED algorithm are able to distribute dots or dot clusters aperiodically, homogeneously, and isotropically for all gray levels. The spectrum of its halftoning result of a constant gray level patch is always isotropic even for midtone gray levels. Since there is no aliasing problem, the directional artifacts and regular structure patterns caused by aliasing can be eliminated.

Simulation results showed that the proposed TDED algorithm can provide a better performance as compared with other error diffusion-based algorithm[3–5,31–33] in terms of RAPSD and anisotropy. When processing real images, its halftoning outputs do not present visible directional artifacts such as worm artifacts, regular structure patterns such as checkerboard patterns, sharpening effects such as edge overshoots, and the mixtures of these artifacts such as false contouring artifacts.

Acknowledgments

The work described in this paper is substantially supported by a grant from the Research Grant Council of the Hong Kong Special Administrative Region, China (Project No: PolyU5120/13E).

References

1. J. C. Stoffel and J. F. Moreland, "A survey of electronic techniques for pictorial reproduction," *IEEE Trans. Commun.* **29**, 1898–1925 (1981).
2. R. W. Floyd and L. Steinberg, "An adaptive algorithm for spatial grey scale," in *Proc. Dig. SID Int. Symp.*, pp. 36–37, Los Angeles, California (1975).
3. R. W. Floyd and L. Steinberg, "An adaptive algorithm for spatial grey-scale," *Proc. Soc. Inf. Disp.* **17**(2), 75–77 (1976).
4. J. Jarvis and C. Roberts, "A new technique for displaying continuous tone images on a bilevel display," *IEEE Trans. Commun.* **24**(8), 891–898 (1976).
5. P. Stucki, "MECCA—a multiple-error correcting computation algorithm for bilevel hardcopy reproduction," *IBM Res. Lab.*, Zurich, Switzerland, Res. Rep. RZ1060 (1981).
6. M. Analoui and J. P. Allebach, "Model-based halftoning using direct binary search," *Proc. SPIE* **1666**, 96–108 (1992).
7. J. B. Mulligan and A. J. Ahumada Jr., "Principled halftoning based on human vision models," *Proc. SPIE* **1666**, 109–121 (1992).
8. T. N. Pappas and D. L. Neuhoff, "Least-squares model-based halftoning," *Proc. SPIE* **1666**, 165–176 (1992).
9. R. A. Ulichney, *Digital Halftoning*, MIT Press, Cambridge, Massachusetts (1987).
10. L. Velho and J. M. Gomes, "Digital halftoning with space filling curves," *Comput. Graph.* **25**(4), 81–90 (1991).
11. I. H. Witten and R. M. Neal, "Using Peano curves for bilevel display of continuous-tone images," *IEEE Comput. Graph. Appl.* **2**, 47–52 (1982).
12. D. E. Knuth, "Digital halftones by dot diffusion," *ACM Trans. Graph.* **6**(4), 245–273 (1987).
13. M. Mese and P. P. Vaidyanathan, "Optimized halftoning using dot diffusion and methods for inverse halftoning," *IEEE Trans. Image Process.* **9**, 691–709 (2000).
14. Y. Zhou et al., "Jumping scanning path error diffusion: a novel halftoning algorithm improving mid-tone quality," in *Proc. of the 2011 Workshop on Digital Media and Digital Content Management*, pp. 215–222 (2011).
15. Z. Fan, "Error diffusion with a more symmetric error distribution," *Proc. SPIE* **2179**, 150–158 (1994).
16. R. A. Ulichney, "Dithering with blue noise," *Proc. IEEE* **76**(1), 56–79 (1988).
17. R. Eschbach and K. T. Knox, "Error-diffusion algorithm with edge enhancement," *J. Opt. Soc. Am. A* **8**(12), 1844–1850 (1991).
18. K. T. Knox and R. Eschbach, "Threshold modulation in error diffusion," *J. Electron. Imaging* **2**(3), 185–192 (1993).
19. T. D. Kite, B. L. Evans, and A. C. Bovik, "Modeling and quality assessment of halftoning by error diffusion," *IEEE Trans. Image Process.* **9**, 909–922 (2000).
20. R. Eschbach, "Error diffusion algorithm with homogeneous response in highlight and shadow areas," *J. Electron. Imaging* **6**, 348–356 (1997).
21. C. Billotet-Hoffmann and O. Bryngdahl, "On the error diffusion technique for electronic halftoning," *Proc. Soc. Inf. Disp.* **24**(3), 253–258 (1983).
22. R. L. Miller and C. M. Smith, "Image processor with error diffusion modulated threshold matrix," U.S. Patent No. 5,150,429 (1992).
23. J. Shiau and Z. Fan, "A set of easily implementable coefficients in error diffusion with reduced worm artifacts," *Proc. SPIE* **2658**, 222–225 (1996).
24. B. W. Kolpatzik and C. A. Bouman, "Optimized error diffusion for image display," *J. Electron. Imaging* **1**(3), 277–292 (1992).
25. P. W. Wong, "Adaptive error diffusion and its application in multiresolution rendering," *IEEE Trans. Image Process.* **5**, 1184–1196 (1996).
26. N. Damera-Venkata and B. L. Evans, "Adaptive threshold modulation for error diffusion halftoning," *IEEE Trans. Image Process.* **10**, 104–116 (2001).
27. R. Levien, "Output dependent feedback in error diffusion halftoning," in *Proc. IS&T 46th Annu. Conf.*, Cambridge, Massachusetts, pp. 115–118 (1993).
28. J. Sullivan, R. Miller, and G. Pios, "Image halftoning using a visual model in error diffusion," *J. Opt. Soc. Am. A* **10**(8), 1714–1724 (1993).
29. R. Eschbach, "Reduction of artifacts in error diffusion by means of input-dependent weights," *J. Electron. Imaging* **2**(4), 352–358 (1993).
30. P. W. Wong and J. P. Allebach, "Optimum error diffusion kernel design," *Proc. SPIE* **3018**, 236–242 (1997).
31. V. Ostromoukhov, "A simple and efficient error-diffusion algorithm," in *Proc. SIGGRAPH*, pp. 567–572 (2001).
32. P. Li and J. P. Allebach, "Tone-dependent error diffusion," *IEEE Trans. Image Process.* **13**, 201–215 (2004).
33. J. Hwang et al., "An optimum design of error diffusion filters using the blue noise in all gray levels," *IEICE Trans. Fundamentals Electron. Commun. Comput. Sci.* **E93-A**(8), 1465–1475 (2010).
34. B. Zhou and X. Fang, "Improving mid-tone quality of variable-coefficient error diffusion using threshold modulation," *ACM Trans. Graph.* **22**, 437–444 (2003).
35. D. L. Lau and R. A. Ulichney, "Blue-noise halftoning for hexagonal grids," *IEEE Trans. Image Process.* **15**(5), 1270–1284 (2006).
36. Y. H. Fung and Y. H. Chan, "Tone-dependent noise model for high quality halftones," *J. Electron. Imaging* **22**(2), 023004 (2013).
37. D. E. Goldberg, *Genetic Algorithms in Search, Optimization and Machine Learning*, 1st ed., Addison-Wesley Longman Publishing Co., Inc., Boston, Massachusetts (1989).
38. S. Kirkpatrick, Jr., C. D. Gelatt, and M. P. Vecchi, "Optimization by simulated annealing," *Science* **220**(4598), 671–680 (1983).

Yik-Hing Fung received the BEng (Hons.) degree and PhD from HKPU in 2000 and 2006, respectively. He was with ASM Pacific Technology Ltd. as an R&D engineer working for computer vision. He was with the Department of Computer Science, Hong Kong Baptist University as a postdoctoral teaching fellow. He is currently working in HKPU. His research interests include digital halftoning, computer vision, image restoration, and compression.

Yuk-Hee Chan received his BSc degree with honors in electronics from Chinese University of Hong Kong in 1987 and his PhD in signal processing from Hong Kong Polytechnic University (HKPU) in 1992. He joined this university in 1992 and is now an associate professor in the Department of Electronic & Information Engineering. He has published over 145 research papers in various international journals and conferences. His research interests include image and video compression, image restoration, halftoning, demosaicking, and fast computational algorithms in digital signal processing. He was the chair of the IEEE Hong Kong Section in 2015.

Downloaded From: https://www.spiedigitallibrary.org/journals/Journal-of-Electronic-Imaging on 09 Nov 2022
Terms of Use: https://www.spiedigitallibrary.org/terms-of-use